Article

Fe and Co-doped (Ba, Ca)TiO₃ Perovskite as Potential Electrocatalysts for Glutamate Sensing

Nicha Sato[1,a], **Makito Haruta**[2,b]**, Kiyotaka Sasagawa**[2,c]**, Jun Ohta**[2,d],
and Oratai Jongprateep[1,3,e]

1 Department of Materials Engineering, Faculty of Engineering, Kasetsart University, Bangkok, Thailand
2 Division of Materials Science, Nara Institute of Science and Technology, Nara, Japan
3 Materials Innovation Center, Faculty of Engineering, Kasetsart University, Bangkok, Thailand
Email: [a]nicha.sat@ku.th, [b]m-haruta@ms.naist.jp, [c]sasagawa@ms.naist.jp, [d]ohta@ms.naist.jp,
[e]fengotj@ku.ac.th (Corresponding author)

Abstract. Barium titanate (BaTiO₃) and calcium titanate (CaTiO₃) are renown perovskite-structured dielectric materials. Nevertheless, utilization of BaTiO₃ and CaTiO₃ in sensing applications has not been extensive. This study, therefore, aims at examining potential usage of BaTiO₃ and CaTiO₃ as enzyme-less sensors. BaTiO₃, CaTiO₃, Fe-doped BaTiO₃, Co-doped BaTiO₃, Fe-doped CaTiO₃, and Co-doped CaTiO₃ (with Fe and Co 5 at%) were synthesized by solution combustion technique, compositionally and microstructurally examined, and tested for their electrocatalytic activities. All powders consisted of submicrometer-sized particles. Measurements of electrocatalytic activities in 0.01 M glutamate solution by cyclic voltammetry were performed. It was found that oxidation peaks occurred at applied voltage close to 0.6 V. Peak currents, which denoted electrocatalytic performance, were prominent in doped powders. Electrocatalytic activities of the powders were discussed with respect to chemical composition, microstructure, and electronic characteristics of the materials.

Keywords: Barium titanate, calcium titanate, doping, electrocatalysis, glutamate, electrochemical sensor.

1. Introduction

Owing to their unique dielectric properties, perovskite materials such as barium titanate ($BaTiO_3$) and calcium titanate ($CaTiO_3$) are extensively exploited in applications such as capacitors, resonators, and electronic devices [1-3]. In addition to prominent dielectric properties, catalytic activity and chemical stability are also observed in perovskite materials [4]. According to Dai et al., $SrTiO_3$ perovskite ceramics exhibited electrochemical activities with glucose oxidase. With the acceptable catalytic performance, $BaTiO_3$ and $CaTiO_3$ are reported to be candidates for electrochemical and sensing material [5-6]. It is generally accepted that chemical composition, doping and microstructure are factors contributing to alteration of electrocatalysis.

As reported by Lee et al., excessive doping of perovskite ceramics, which leads to formation of secondary phase, was reported to deteriorate electrocatalysis. However, proper doping of the $BaTiO_3$ or $CaTiO_3$ perovskite by divalent and/or trivalent ions introduces lattice distortions and oxygen vacancies. The oxygen vacancies are generally accepted as defects that promote charge carriers and ionic conductivity [7].

Microstructural control was reported to affect electrocatalysis. According to Zhang et al., electrocatalytic activities for the reactions were observed in small-particulate sensing materials [8]. Owing to high surface areas and abundant active sites, peak currents for oxidation reactions increase. It was also reported that fine particles accommodated transportation of electrogenerated carriers to the surface, which consequently led to high mass transfer. Not only does particles size contribute to better catalysis, proper interparticle distances are also beneficial to electrocatalytic activities.

According to Perez et al., ratio of interparticle distances to particle size can be crucial to electrocatalysis. As interparticle distance to particle size ratio decreases, diffusion characteristic of the reaction alters from the spherical diffusion of isolated particles to planar diffusion [9]. This lead to diminished active area and catalysis activities [10-11]

Electronic structure, specifically of bandgap energy of the perovskite oxide, also affects electrocatalytic activity. In general, narrow bandgap promotes electron transfer from bulk to surface of catalyst, which results in reduction of the activation energy for electrocatalytic activity [12].

Through enhancement of electrocatalysis in perovskite materials, their electrochemical sensing efficacy is achieved. With extensive concern regarding food quality and safety, development of food sensors becomes increasingly vital. One of the ubiquitous food additives used as a flavoring ingredient is monosodium glutamate (MSG) [13]. It has been reported that enhanced flavor is generally found in food containing 0.1-0.8 wt% glutamate concentrations, whereas a decline in flavor sensing is observed in the food with more than 1 wt% of glutamate concentration [14-15]. In addition to flavor enhancement, glutamate is also reported to function as an excitatory neurotransmitter. Concentrations of glutamate in human brains are in the range between 1 and 300 µM [16]. Nevertheless, excessive glutamate concentration in brains can be detrimental. Based on numerous scientific evidences, high doses of glutamate in the synaptic cleft result in neurological disorders such as Alzheimer, Parkinson's diseases, and depression [17-18]. Additionally, since severe adverse reactions to glutamate were continually reported in people who are particularly sensitive to food additives, detection of glutamate becomes crucial.

This study aims at examining potential usage of Fe and Co-doped (Ba, Ca)TiO_3 as glutamate sensors. Electrocatalytic activities of the materials which indicate the sensing potential, were investigated and discussed with respect to chemical composition, microstructure and bandgap energy.

2. Experimental Procedures

Barium titanate, calcium titanate as well as barium titanate and calcium titanate doped with 5 at% of Fe and Co were synthesized by solution combustion technique. Barium nitrate ($Ba(NO_3)_2$, Deajung), calcium nitrate ($Ca(NO_3)_2 \cdot 4H_2O$, Deajung), iron (III) nitrate ($Fe(NO_3)_3 \cdot 9H_2O$, Deajung), cobalt (II) nitrate ($Co(NO_3)_2$, Univar), and titanium dioxide (TiO_2, Sigma-Aldrich) in nitric acid (HNO_3, Univar), were mixed together to form an aqueous solution. Glycine (NH_2CH_2COOH, Deajung), was added to the prepared solution to accommodate the combustion process, which occurred at the temperature close to 400°C. The powders obtained from the solution combustion process were subsequently calcined at 900°C for 3 hours.

Chemical composition and microstructural analysis of the calcined powder were conducted using an x-ray diffractometer (Philips, X'Pert). The measurements were conducted at the 2 theta angle ranging from 20° to 80°, with the scanning rate and step sizes of 0.7°/min and 0.02°. Particle morphology was examined by a

scanning electron microscope (FEI, Quanta 450). An Image J software was employed in particle size analysis, whereas a Brunauer-Emmett-Teller (Micrometics, 3Flex) was utilized in the measurements of the specific surface area of the powders.

A UV-Vis spectrophotometer (UV-1700) was exploited in determination of optical bandgap energies of the synthesized powders. The measurements of optical transmission were conducted within the wavelength ranging between 300 and 900 nanometers. The value of optical bandgap is expressed by the following Eq. (1):

$$Eg = h\nu/e = hc/e\lambda \tag{1}$$

where Eg is the bandgap energy (eV), h is the Planck's constant (Js), c is the speed of light (m/s), e is the electron charge (C) and λ is the wavelength of the light.

Cyclic voltammetry technique was used in determination of electrocatalytic activities of the powders. The measurements were conducted using Metrohm AutoLab Potentiostat (PGSTAT302N). The synthesized powders were impregnated into multi-walled carbon nanotube (MWCNT) at the weight ratio of powder to MWCNT equal to 1:1. The powder/MWCNT composites were painted onto the working electrode with the area of 5 mm * 5 mm. Voltages ranging between -0.8 to 0.8 V at the scan rate of 0.05 V/s were applied to the electrodes. Pt and Ag/AgCl were used as the counter electrode and the reference electrode, respectively. The working electrode was activated in 0.1 M sodium hydroxide solution. Detection of glutamate was conducted in 0.01 M L-glutamic acid monosodium salt monohydrate, $(C_5H_8NNO_4 \cdot H_2O)$ (98+% Alfa Aesar).

3. Results and Discussion

3.1. Phase Identification

Phase identification analysis of $BaTiO_3$, $CaTiO_3$, $BaTiO_3$ and $CaTiO_3$ powders doped with 5 at% Co and Fe were conducted through the x-ray diffraction technique (XRD). The results revealed that all powders contained a single phase, which is commonly observed in the powders synthesized by the solution combustion technique. The XRD results, as shown in Fig. 1, indicated that the diffraction patterns of the $BaTiO_3$ system corresponded to barium titanate ($BaTiO_3$, JCPDS 075-0561). For the $CaTiO_3$ system, the diffraction patterns corresponded to calcium titanate ($CaTiO_3$, JCPDS 076-2400), as shown in Fig. 1. No secondary phase was observed even in the powders with Co and Fe doping.

A similar observation related to single phase formation was reported by Y. Liu et al. It was reported that a single phase $SrTiO_3$ was present at doping concentration as high as 50 mol% Fe. For the Co doped $SrTiO_3$, the single phase still existed as Co doping content increased to 50 mol%. According to S. Qiu et al. and A. Murashkina et al. homogenous solid solution can be obtained in Fe doped $BaTiO_3$ system at the doping concentration ranging from 20 to 50 mol% [16-18].

Results from the current study suggested that extensive metal substitutional upon doping was possible in the $BaTiO_3$ and $CaTiO_3$ systems. Considering an atomic size factor, it was generally accepted that high solid solubility can be achieved when the atomic radii of the solvent differ from that of the solute by less than 15% [19].

In the system of Fe-doped $(Ba, Ca)TiO_3$, Fe^{3+} commonly substitutes into Ti^{4+} sites [20]. Since the ionic radii of Fe^{3+} and Ti^{4+} are 0.79Å and 0.75 Å, respectively, small difference in solute/solvent ionic radii of 5.33% accommodate complete substitution, leading to chemical homogeneity of the solid solution. For the Co-doped $(Ba, Ca)TiO_3$, Co^{2+} commonly substitute into Ti^{4+} sites. With minimal ionic radii difference of 1.35 %, formation of single-phase was also observed.
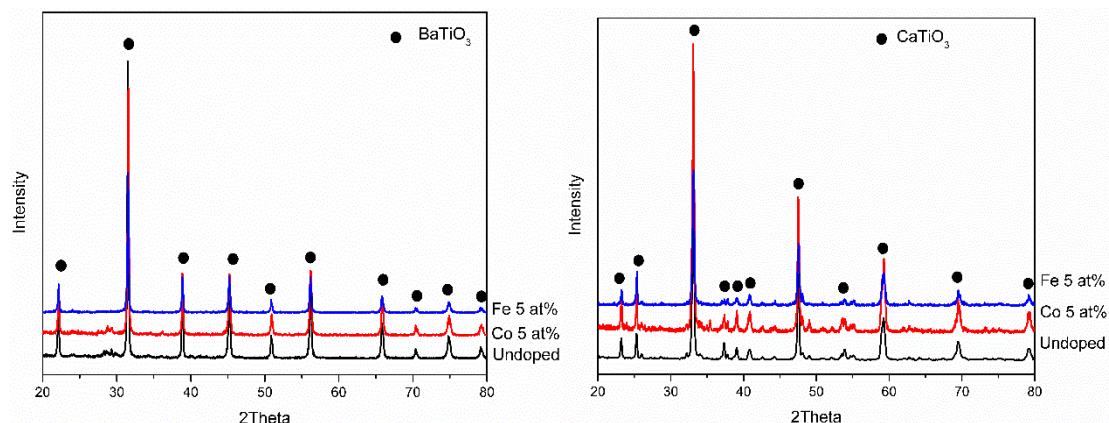
Fig. 1.   XRD patterns of undoped, barium titanate and calcium titanate doped with 5 at% Co, 5 at% Fe.

3.2. Microstructure and Specific Surface Area

The secondary electron mode in a scanning electron microscope was employed in examination of microstructure of the powders synthesized by solution combustion technique as shown in Fig. 2. The synthesized powders contained equiaxial particles with average sizes ranging from 0.18 ± 0.05 to 0.57 ± 0.12 micrometer.
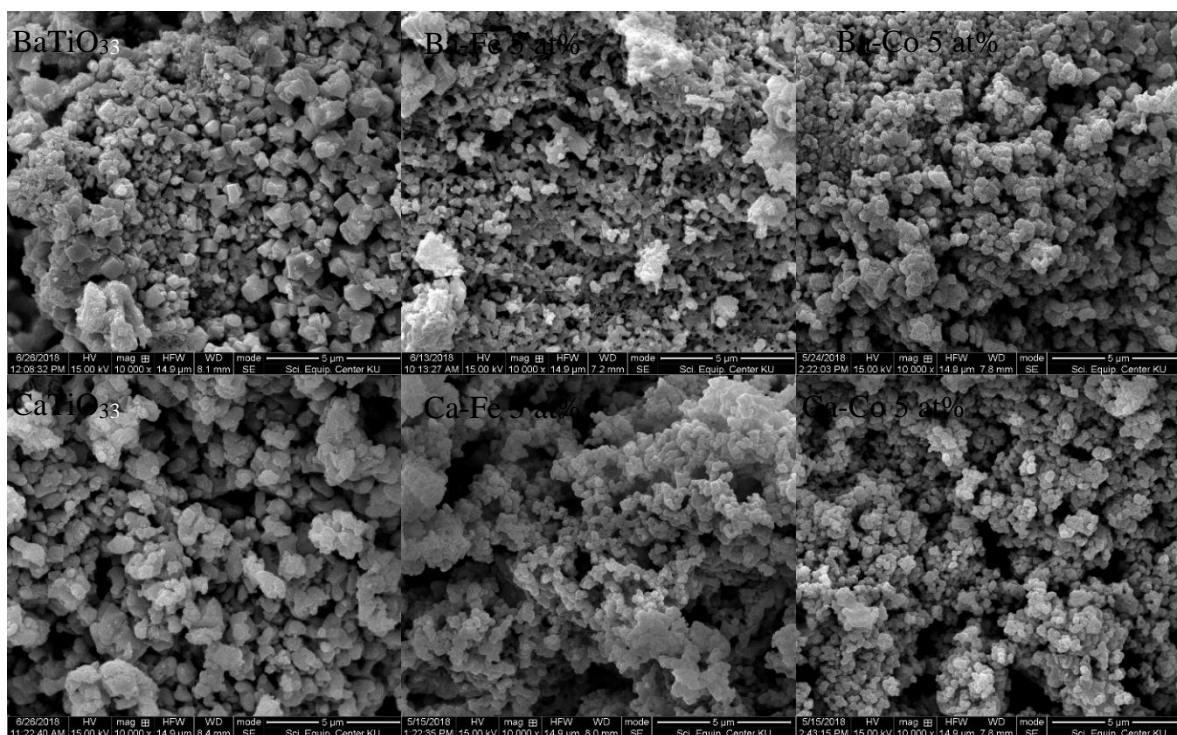

Fig. 2.   SEM micrographs showing particle morphology of powders synthesized by solution combustion technique with following compositions: (a) BaTiO₃, (b) BaTiO₃ doped 5 at% Fe (c) BaTiO₃ doped 5 at% Co, (d) CaTiO₃, (e) CaTiO₃ doped 5 at% Fe and (f) CaTiO₃ doped 5 at% Co

As average particle sizes of the Fe-doped BaTiO₃ (or CaTiO₃) and Co-doped BaTiO₃ (or CaTiO₃) were in close proximity, the results revealed that types of dopants did not significantly affect particle size. Nevertheless, compared with undoped powders, discernable particle refinement occurred as a result of doping.

It was found that doping led to defect formation such as oxygen vacancies. Equations (Eq. (2)-(3)) representing doping of Fe^{3+} and Co^{2+} into Ti^{4+} site in a perovskite structure may be expressed as follows [21-22]:

$$Fe_2O_3 \leftrightarrow 2Fe_{Ti}' + V_O^{\cdot\cdot} + 3O_O^X \tag{2}$$

$$Co^{2+}_{Ti^{4+}} \leftrightarrow Co''_{Ti^{4+}} + V_O^{\cdot\cdot} \tag{3}$$

Oxygen vacancy has been reported to create disorder in the crystalline structure as well as lattice distortions. Reduction in periodicity in the lattice disrupts crystal continuity and diminishes crystal growth [23-25]. Ohno et al., also reported that lower crystal growth was observed in the doped powders. As oxygen vacancies were created, pining sites which lead to the decrease of ion mobility were generated. Low ion mobility also caused the crystal growth inhibition [26].

Specific surface areas (SSA) of the synthesized powders were examined. As shown in Table 1, values of SSA measured by the Brunauer-Emmett-Teller (BET) technique ranged between 4.998 and 6.39 m^2/g. No significant difference in specific surface area between the undoped and doped powders was observed. In general, non-agglomerated fine particles tend to have a high surface area. In this study, even though particle refinement was observed in the doped powders, specific surface area values of the doped powders were in comparable range with those of the undoped powders. This observation suggested that doped powders exhibited a greater degree of agglomeration. An observation related to agglomeration in Fe-doped $(Ba,Ca)TiO_3$ powders was reported. According to Keswani et al. and Medeiros et al., an increase in agglomeration was attributed to highly reactive nature of Fe ions [27-28].

Table 1.   Particle size and specific surface area of $BaTiO_3$ and $CaTiO_3$ doped with Fe and Co.

Composition	Particle size (μm)			SSA (m^2/g)		
	Undoped	Fe 5 at%	Co 5 at%	Undoped	Fe 5 at%	Co 5 at%
$BaTiO_3$	0.57 ± 0.12	0.23 ± 0.06	0.23 ± 0.06	5.22	4.99	6.39
$CaTiO_3$	0.40 ± 0.01	0.18 ± 0.04	0.18 ± 0.05	5.99	6.19	5.51

Size uniformity with narrower particle size distribution were also observed in Fe and Co-doped $BaTiO_3$ and $CaTiO_3$ powders, as shown in Fig. 3. It has been reported that uniform particle size can result in enhanced electrocatalytic activity. Higher activity and stability, commonly observed in powders with narrow particle size distribution, are attributed to the fact that coarsen particles with low activity are rarely present in the powders with size uniformity [29]. Results related to particle size distribution therefore suggested that improved electrocatalytic performance might occur in doped powders [30-31].
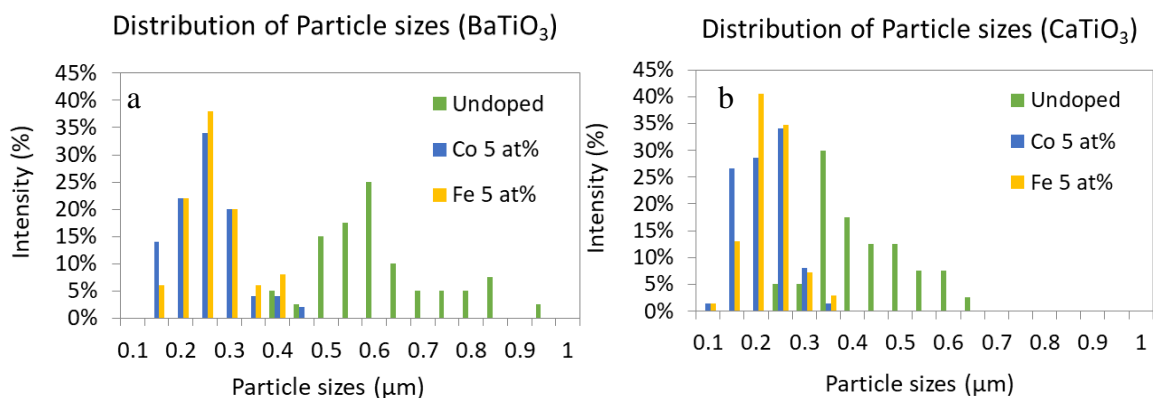

Fig. 3.   Particle size distribution of (a) $BaTiO_3$ and (b) $CaTiO_3$ powder synthesized by solution combustion technique

3.3. Bandgap Energy

UV-Vis Spectrometry technique was employed in determination of bandgap energy. Bandgap values of synthesized powders were calculated according to Eq. (1). As shown in tauc plots (Fig. 4.), bandgap energy values of the $BaTiO_3$ powder slightly decreased from 3.17 eV for $BaTiO_3$ to 3.14 eV and 3.15 eV as the powder was doped with 5 at% of Fe and Co, respectively. A similar result was observed in the $CaTiO_3$ system. Bandgap energy reduced from 3.18 eV to 3.08 and 2.88 eV as the $CaTiO_3$ was doped with Fe and Co, respectively.
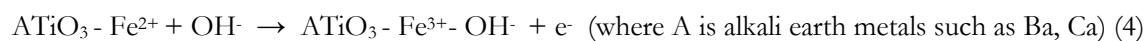
The results suggested that doping could result in slight minimization of bandgap energy. The observation was being agreed with various findings previously reported. According to A. Rothschild et al. and C.W. Bark et al., Co-doped $BiTiO_3$ and Fe-doped $SrTiO_3$ exhibited bandgap energy reduction [32-34].

Bandgap narrowing in metal doped ceramics has been reported to be associated with formation of a new dopant energy level below the conduction band and upward shift of the valence band edge. According to Z. Chao et al., bandgap reduction of Fe-doped $BaTiO_3$ and $SrTiO_3$ powders was associated with formation of the impurity states due to oxygen vacancies below the conduction band and Fe doping level above the valence band edge [35]. An upward shift of the valence band edge in $PbSrTi_{1-x}Fe_xO_3$ was also reported by Pontes et al. According to Y.W. Li et al., doping Co in perovskite-structure ceramics also exhibits a decline of the conduction band bottom which results in bandgap energy reduction [36-37].

3.4. Electrocatalytic Activity

Electrocatalytic activities of the powder were examined by cyclic voltammetry technique as shown in Fig. 5. the I-V measurements of the synthesized powder in glutamate solution demonstrated peak currents corresponding to oxidation reactions at applied voltage close to 0.6 V. Oxidation peak occurring as a result of multiwalled carbon nanotubes (MWCNTs) reaction with the solution were evident at 0.2 V. A similar observation was reported in the study related to electrocatalytic properties of MWCNTs/polypyrrole composite [38].

Potential oxidation reactions related to glutamate detection by Fe-doped perovskite materials can be expressed by Eq. (4) – (6): [39-40]

$$ATiO_3 - Fe^{2+} + OH^- \rightarrow ATiO_3 - Fe^{3+} - OH^- + e^- \text{ (where A is alkali earth metals such as Ba, Ca)} \quad (4)$$
$$ATiO_3 - Fe^{3+} + \text{L-glutamate} + O_2 + H_2O \rightarrow ATiO_3 - Fe^{2+} + 2 \text{ ketoglutarate} + H_2O_2 \quad (5)$$
$$H_2O_2 \rightarrow 2H^+ + O_2 + 2e^- \quad (6)$$

In the current study, $BaTiO_3$, Fe-doped $BaTiO_3$ and Co doped $BaTiO_3$ exhibited oxidation peak currents of 0.262, 0.609, and 0.508 mA, respectively. For the $CaTiO_3$, Fe doped $CaTiO_3$ and Co doped $CaTiO_3$, oxidation peak currents of 0.052, 0.249, and 0.229 mA were detected, respectively, as shown in Table 3. The results suggested that enhancement of electrocatalytic activity could be achieved through doping.

It has been reported that electrochemical reactions of the electrode are associated with electron exchange reactions between neighbouring redox sites (electron hopping effect) and electronic conduction [41]. Enhancement of electrocatalytic activity via electron hopping effect was reported in metal oxide doped by transition elements such as Co^{2+}, Fe^{3+}, Mn^{3+}, Zn^{2+}, Ni^{2+}, and Cu^{2+} [42-44]. It was also reported that the electron hopping abilities are dependent on electron transfer properties [45-46]. In addition, enhanced electron transfer from bulk to surface of catalyst also results in reduction of the activation energy for electrocatalytic activity [47].

For these reasons, doping of $BaTiO_3$ and $CaTiO_3$ by Fe and Co, which results in bandgap narrowing and enhanced electron transfer, could exhibit improved electrocatalytic performance. Observations from this study were being agreed with the study reported by B. Sawicki et al. and Y. Wang et al., which stated that lower bandgap improve the electrocatalytic activity [48-49].

The cyclic voltammograms also revealed peaks associated with reduction reactions. In this study, the ratio of oxidation peak current to reduction peak current ranged from 0.2 to 0.54. With the ratio lower than unity, the results suggested quasi-reversible reactions [50]. Since the irreversible systems generally yield products that are incapable of converting back to the original reactants, a reversible system is preferred to the irreversible one [51]. According to E.P. Randviir et al., irreversibility might be attributed to low reaction kinetics and limited electron transfer rate [52].
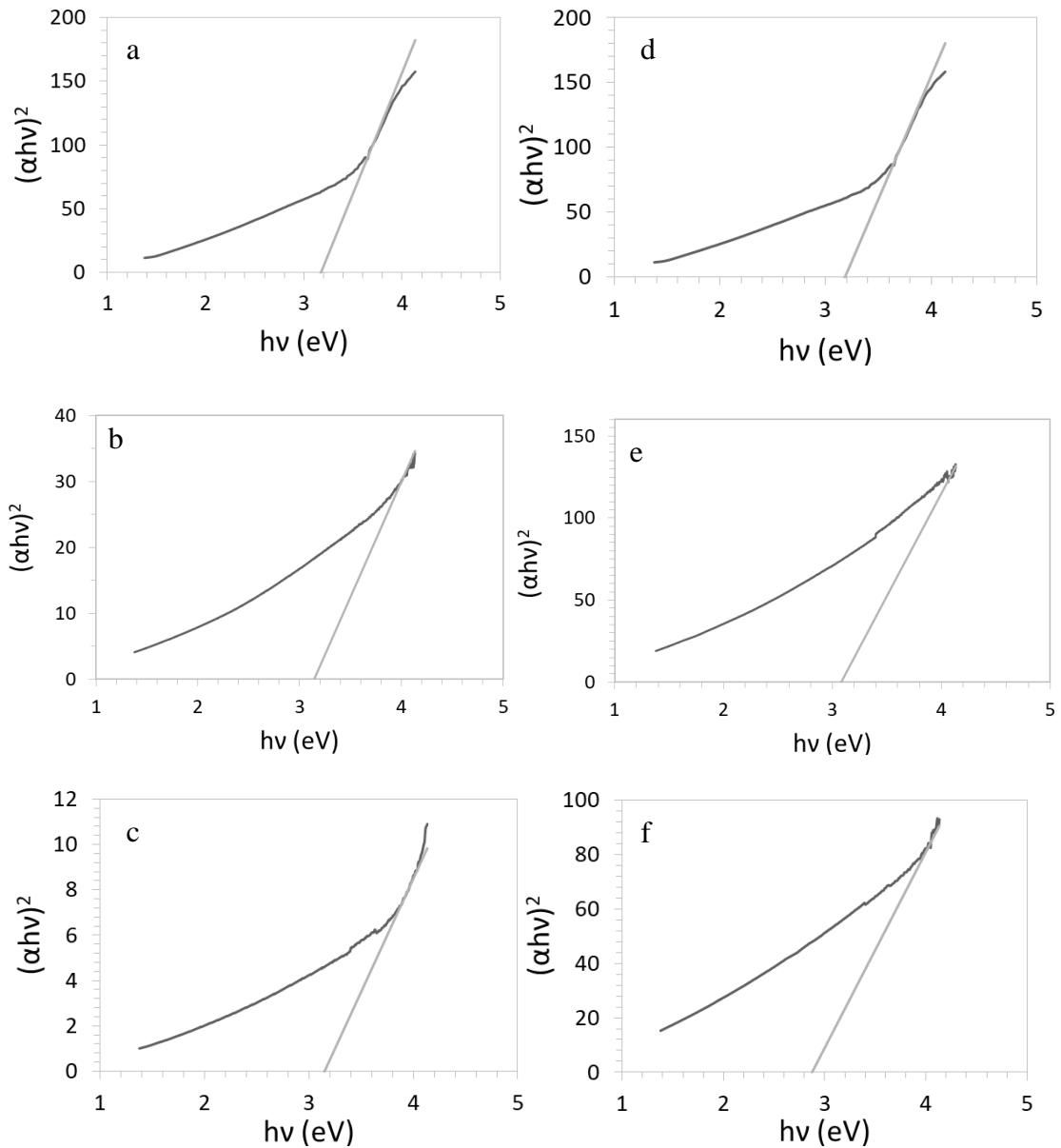
Fig. 4. Tauc plot of synthesized powders with following composition: (a) BaTiO₃, (b) BaTiO₃ doped with 5 at% Fe, (c) BaTiO₃ doped with 5 at% Co, (d) CaTiO₃, (e) CaTiO₃ doped with 5 at% Fe and (f) CaTiO₃ doped with 5 at% Co.

Table 2.   The bandgap energy values of $BaTiO_3$ and $CaTiO_3$ doped with Fe and Co.

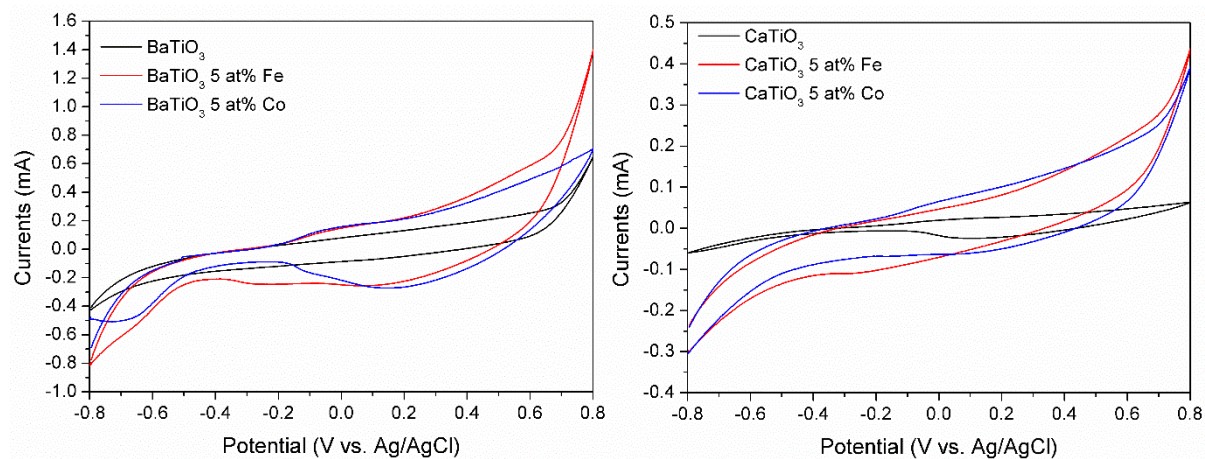| Composition	Band gap energy (eV)		
	Undoped	Fe 5 at%	Co 5 at%
$BaTiO_3$	3.17	3.14	3.15
$CaTiO_3$	3.18	3.08	2.83

Fig. 5. Cyclic voltammogram of BaTiO₃ and CaTiO₃ doped with 5 at% Fe and 5 at% Co, measured in glutamate solution with concentration of 0.01M.

Table 3. Peak current of BaTiO₃ and CaTiO₃ doped with 5 at% Fe and Co measured in glutamate solution.

Compositions	Peak current (I_p) (mA)	
	Oxidation	Reduction
BaTiO₃	0.262	0.064
BaTiO₃ doped 5 at% Fe	0.609	0.256
BaTiO₃ doped 5 at% Co	0.508	0.273
CaTiO₃	0.052	0.024
CaTiO₃ doped 5 at% Fe	0.249	0.050
CaTiO₃ doped 5 at% Co	0.229	0.060

Since Fe and Co doped powders exhibited superior performance in electrocatalytic measurements, Fe-doped BaTiO₃, Co doped BaTiO₃, Fe-doped CaTiO₃ and Co doped CaTiO₃ were employed in determination of sensitivity of glutamate detection. Relationships between current density (J) and concentration of glutamate solution in concentrations ranging from 0.1 to 100 mM, were shown in Fig. 6. The equations representing the current densities and solution concentration as well as R^2 values in various ranges of concentrations were expressed in Table 4. According to Table 4, all R^2 values ranged from 0.76 to 0.98, which exceed the accepted value of 0.75 [53]. The overall results, hence, suggested that current densities and glutamate concentration exhibited good linear relationship.

The relationship between current density and glutamate concentrations, specifically slopes of the calibration curves, were employed in determination of sensitivity of the detection. The results, as shown in Table 4, indicated sensitivity values in the range between 8.2×10^{-4} and 3.1×10^{-2} mA/(mMcm²). It was found that superior sensitivity values were observed at low concentration detection. This observation was being agreed with the study reported by N. Shen et al., According to M. Metto et al., at high analyte concentrations, surface deactivation originated by competitive adsorption of reaction products was possible. Limited reactive surface subsequently led to diminished electrochemical reactions [54-55].

Sensitivity results obtained from the current study were in comparable ranges with the results previously reported. Good linear relationship between J (current density)-vs-C (concentration) was also observed. With acceptable detection sensitivity at various concentration ranges, the findings suggested that Fe-doped BaTiO₃, Co doped BaTiO₃, Fe-doped CaTiO₃ and Co doped CaTiO₃ have potential usage for glutamate sensing.
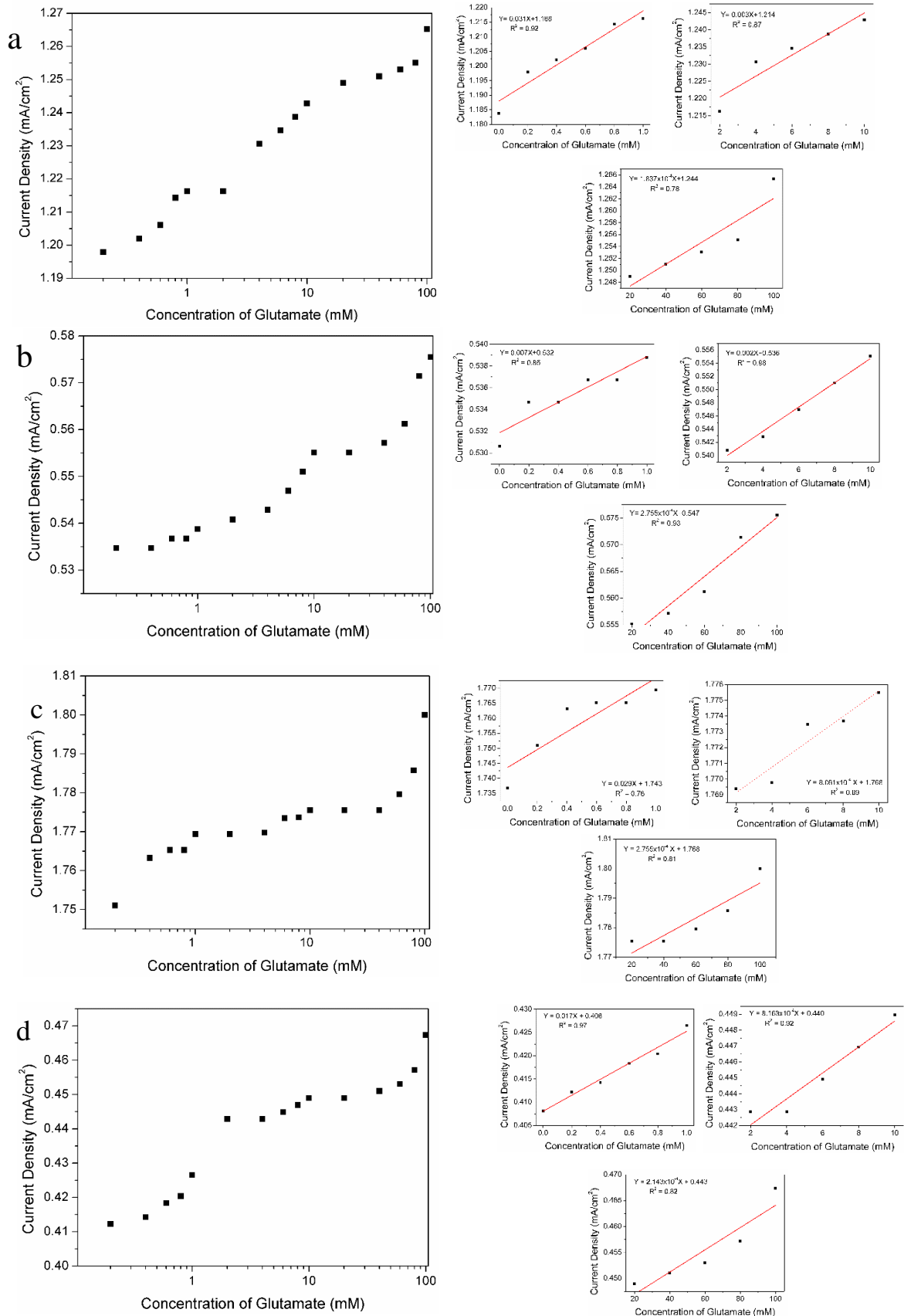
Fig. 6.   (Left) Relationships between current density (J) and glutamate solution concentration (in log-scale), and (Right) calibration curves of the powders with following compositions: (a) BaTiO$_3$ doped 5 at% Fe, (b) BaTiO$_3$ doped 5 at% Co, (c) CaTiO$_3$ doped 5 at% Fe and (d) CaTiO$_3$ doped 5 at% Co.

Table 4.   Sensitivity of BaTiO$_3$, CaTiO$_3$ doped with Fe, Co 5 at% when measured in glutamate solution.

Compositions	Concentration of glutamate (mM)	Equations Representing Current Density (J)	R^2	Sensitivity (mA mM^{-1}cm^{-2})
BaTiO$_3$ doped 5 at% Fe	0-1	J= 0.031C+1.188	0.92	3.1x10^{-2}
	1-10	J= 0.003C+1.214	0.87	3x10^{-3}
	10-100	J=1.837x10^{-4}C + 1.244	0.78	1.837x10^{-4}
BaTiO$_3$ doped 5 at% Co	0-1	J= 0.007C+0.532	0.85	7x10^{-3}
	1-10	J= 0.002C+0.536	0.98	2x10^{-3}
	10-100	J=2.755x10^{-4}C + 0.547	0.93	2.755x10^{-4}
CaTiO$_3$ doped 5 at% Fe	0-1	J= 0.029C+1.743	0.76	2.9x10^{-2}
	1-10	J=8.061x10^{-4}C + 1.768	0.89	8.061x10^{-4}
	10-100	J=2.755x10^{-4}C + 1.768	0.81	2.755x10^{-4}
CaTiO$_3$ doped 5 at% Co	0-1	J= 0.017C+0.408	0.97	1.7x10^{-2}
	1-10	J=8.163x10^{-4}C + 0.440	0.92	8.163x10^{-4}
	10-100	J=2.143x10^{-4}C + 0.443	0.82	2.143x10^{-4}

Table 5.   Performance of glutamate detection, measured by various types of electrodes.

Electrodes	Concentration range (mM)	Sensitivity (mA mM^{-1}cm^{-2})	Ref.
CNT	0.05-5	0.71x10^{-4}	[56]
Pt/ta-C/APTES/GlOx	0.01-5	2.9x10^{-3}	[57]
CeO$_2$/TiO$_2$/GmOx/Chit/o-PD/Pt	0.005-0.05	3.95 x10^{-4}	[58]
Au	0.25-2.7	3.4 x10^{-2}	[59]
Co$_3$O$_4$/GCE	10^{-5} - 100	9.5x10^{-5}	[60]

4.   Conclusions

Barium titanate and calcium titanate and barium titanate and calcium titanate doped with 5 at% Fe and Co powders were successfully synthesized by a solution combustion technique. Fine particles with average sizes smaller than 0.6 micrometer were attained. Effects of Fe and Co doping on phase homogeneity, microstructure, and bandgap energy were examined. Experimental results revealed that homogeneous single phase remained in doped powders, while particle refinement with narrow size distribution, as well as reduction of bandgap energy occurred as a result of doping. Electrocatalytic activities, which revealed sensing ability of the powders, were also examined using cyclic voltammetry technique. Attributed to size uniformity and bandgap narrowing, superior oxidation peak currents were observed in the doped powders. The results also indicated moderate electrocatalytic activities of the synthesized powder in glutamic acid solutions with concentration ranging from 0.1 to 100 mM. Good linear relationship between J (current density)-vs-C (concentration) as well as moderate detection sensitivity at various concentration ranges suggested that Fe-doped BaTiO$_3$, Co doped BaTiO$_3$, Fe-doped CaTiO$_3$ and Co doped CaTiO$_3$ had potential usage for glutamate sensing.

Acknowledgement

References

[1] I. Fujii, M. Ugorek and S. Trolier-McKinstry, "Grain size effect on the dielectric nonlinearity of BaTiO$_3$ ceramics," *J. Appl. Phys.*, vol. 107, p. 104116, May 2010.

[2] L. Padilla-Campos, D. E. Diaz-Droguett, R. Lavín, and S. Fuentes, "Synthesis and structural analysis of Co-doped BaTiO$_3$," *J. Mol. Struct.*, vol. 1099, pp. 502-509, Jul. 2015.

[3] O. Jongprateep and N. Sato, "Effects of synthesis techniques on chemical composition, microstructure and dielectric properties of Mg-doped calcium titanate," in *AIP Conf. Proc.*, April 2018, vol. 1957, no. 1, p. 020002.

[4] N. F. Atta, M. H. Binsabt, E. H. Mel-Ads, and A. Galal, "Synthesis of neodymium-iron nanoperovskite for sensing applications of an antiallergic drug," *Turk. J. Chem.,* vol. 41, pp. 476-492, Feb. 2017.

[5] H. Dai, Y. Zhong, X. Wu, R. Hu, L. Wang, Y. Zhang, G. Fan, X. Hu, J. Li, and Z. Yang, "Synthesis of perovskite-type SrTiO$_3$ nanoparticles for sensitive electrochemical biosensing applications," *J. Elec. Chem.,* vol. 810, pp. 95-99, Jan. 2018.

[6] S. Selvarajan, N. R. Alluri, A. Chandrasekhar, and S. Kim, "BaTiO$_3$ nanoparticles as biomaterial film for self-powered glucose sensor application," *Sens. Actuators, B,* vol. 234, pp. 395-403, May 2016.

[7] S.-Y. Lee, M.-A. Parkm, J.-H. Kim, H. Kim, C.-J. Choi, D.-K. Lee, and K.-S. Ahn, "Enhanced electrocatalytic activity of the annealed Cu$_{2-x}$S counter electrode for quantum dot-sensitized solar cells," *J. Electrochem. Soc.*, vol. 160, no. 11, pp. H847-H851, Oct. 2013.

[8] X.-G. Zhang, T, Arikawa, Y. Murakami, K. Yahikozawa, and Y. Takasu, "Electrocatalytic oxidation of formic acid on ultrafine palladium particles supported on glassy carbon," *Electrochim. Acta*, vol. 40, no. 12, pp. 1889-1897, Jan. 1995.

[9] W. Gu, Y. Song, J. Liu, and F. Wang, "Lanthanum-based compounds: electronic band-gap-dependent electrocatalytic materials for oxygen reduction reaction," *Chem. Eur. J.,* vol. 23, no. 42, pp. 10126-10132, May 2017.

[10] L. Bian, J.-B. Xu, M.-X. Song, F.-Q. Dong, H.-L. Dong, F.-N. Shi, L. Wang, and W. Ren, "Designing perovskite BFO (111) membrane as an electrochemical sensor for detection of amino acids: A simulation study," *J. Mol. Struct.*, vol. 1099, pp. 1-9, Jun. 2015.

[11] R. Devi, S. Gogoi, S. Barua, H. S. Dutta, M. Bordoloi, and R. Khan, "Electrochemical detection of monosodium glutamate in foodstuffs based on Au@MoS$_2$/chitosan modified glassy carbon electrode," *Food Chem.*, vol. 276, pp. 350-357, 2019.

[12] M. S. Rodríguez, M. E. González, and M. E. Centurión, "Determination of monosodium glutamate in meat products," *J. Arg. Chem. Soc.,* vol. 91, pp. 41-45, May 2003.

[13] M. Sarantis and D. Attwell, "Glutamate uptake in mammalian retinal glia is voltage-and potassium-dependent," *Brain Res.,* vol. 516, no. 2, pp. 322–325, May 1990.

[14] S. K. Hamdan and Z. M. Zain "In vivo electrochemical biosensor for brain glutamate detection: A mini review," *Malays. J. Med. Sci.*, no. Special Issue, pp. 12-24, Dec. 2014.

[15] M. Jamal, S. Chakrabarty, M. A. Yousuf, A. Khosla, and K. M. Razeeb, "Micro and nanostructure based electrochemical sensor platform for glutamate detection," *Microsyst. Technol.,* vol. 24, pp. 4193-4206, Jan. 2018.

[16] Y. Liu, S. Baumann, F. Schulze-Küppers, D. N. Mueller, and O. Guillon, "Co and Fe co-doping influence on functional properties of $SrTiO_3$ for use as oxygen transport membranes," *J. Eur. Ceram. Soc.*, vol. 38, pp. 5058-5066, Dec. 2018.

[17] S. Qiu, W. Li, Y. Liu, G. Liu, Y. Wu, and N. Chen, "Phase evolution and room temperature ferroelectric and magnetic properties of Fe-doped $BaTiO_3$ ceramics," *Trans. Nonferrous Met. Soc. China*, vol.20, pp. 1911−1915, Oct. 2010.

[18] A. Murashkina, V. Maragou, D. Medvedev, V. Sergeeva, A. Demin, and P. Tsiakaras, "Single phase materials based on Co-doped $SrTiO_3$ for mixed ionic-electronic conductors applications," *J. Pow. Sour.*, vol. 210 pp. 339-344, Mar. 2012.

[19] W. Hume-Rothery, *Atomic Theory for Students of Metallurgy*, 5th ed. London: The Institute of Metals 1969.

[20] B. Ertuğ, "The overview of the electrical properties of barium titanate," *AJER.*, vol. 2, pp. 1-7, 2013

[21] L. da Silva, J.-C. M'Peko, J. Andre, A. Beltra, L. Gracia, M. I. B. Bernardi, A. Mesquita, E. Antonelli, M. L. Moreira, and V. R. Mastelaro, "Insight into the effects of Fe addition on the local structure and electronic properties of $SrTiO_3$," *J. Phys. Chem. C,* vol. 118, pp. 4930−4940, Jan. 2014.

[22] A. Rani, J. Kolte, and P. Gopalan, "Effect of cobalt substitution on the structural, electrical and magnetic properties of $BaTiO_3$ ceramics," in *IEEE International Symposium on the Applications of Ferroelectric, International Symposium on Integrated Functionalities and Piezoelectric Force Microscopy Workshop, ISAF/ISIF/PFM*, 2015, pp. 171-174.

[23] M. B. Smith, K. Page, T. Siegrist, P. L. Redmond, E. C. Walter, R. Seshadri, L. E. Brus, and M. L. Steigerwald, "Crystal structure and the paraelectric-to-ferroelectric phase transition of nanoscale $BaTiO_3$," *J. Am. Chem. Soc.,* vol. 130, no. 22, pp. 6955-6963, 2008.

[24] H. Liu, K. Zhu, Y. Liu, W. Li, L. Cai, X. Zhu, M. Cheng, and W. Yang, "Structure and electrochemical properties of cobalt-free perovskite cathode materials for intermediate-temperature solid oxide fuel cells," *Electrochim. Acta,* vol. 279, pp. 224-230, May. 2018.

[25] J. Khajonrit, U. Wongpratat, P. Kidkhunthod, S. Pinitsoontorn, and S. Maensiri, "Effects of Co doping on magnetic and electrochemical properties of $BiFeO_3$ nanoparticles," *J. Magn. Magn. Mater.*, vol. 449, pp. 423-434, Mar. 2018.

[26] T. Ohno, S. Ochibe, H. Wachi, S. Hirai, T. Arai, N. Sakamoto, H. Suzuki, and T. Matsuda, "Preparation of metal catalyst component doped perovskite catalyst particle for steam reforming process by chemical solution deposition with partial reduction," *Adv. Pow. Tech.,* vol. 29, pp. 584-589, Mar. 2018.

[27] B. C. Keswani, R. S. Devan, R. C. Kambale, A. R. James, S. Manandhar, Y. D. Kolekar, and C. V. Ramana, "Correlation between structural, magnetic and ferroelectric properties of Fe-doped (Ba-Ca)TiO_3 lead-free piezoelectric," *J. Alloys Compd.,* vol. 712, pp. 320-333, Jul. 2017.

[28] P. N. Medeiros, V. D. Araújo, A. P. A. Marques, R. L. Tranquilin, C. A. Paskocimas, M. R. D. Bomio, J. A. Varela, E. Longo, and F. V. Motta, "Effect of different starting materials on the synthesis of $Ba_{0.8}Ca_{0.2}TiO_3$," *J. Adv. Ceram.,* vol. 4, pp. 65-70, Mar. 2015.

[29] E. Higuchi, A. Taguchi, K. Hayashi, and H. Inoue, "Electrocatalytic activity for oxygen reduction reaction of Pt nanoparticle catalysts with narrow size distribution prepared from $[Pt_3(CO)_3(\mu\text{-}CO)3]_n^{2-}$ (n = 3–8) complexes," *J. Electroanal. Chem.,* vol. 663, pp. 84–89, Dec. 2011.

[30] T. Brülle, W. Ju, P. Niedermayr, A. Denisenko, O. Paschos, O. Schneider, and U. Stimming, "Size-dependent electrocatalytic activity of gold nanoparticles on HOPG and highly boron-doped diamond surfaces," *Molecules*, vol. 16, pp. 10059-10077, Dec. 2011.

[31] S. Mukerjee, "Particle size and structural effects in platinum electrocatalysis," *J. Appl. Electrochem.*, vol. 20, pp. 537-548, 1990.

[32] A. Rothschild, S. J. Litzelman, H. L. Tuller, W. Menesklou, T. Schneider, and E. Ivers-Tiffée, "Temperature-independent resistive oxygen sensors based on $SrTi_{1-x}Fe_xO_{3-\delta}$ solid solutions," *Sens. Actuators, B*, vol. 108, pp. 223-230, 2005.

[33] C. W. Bark, "Structural and optical properties of bandgap engineered bismuth titanate by cobalt doping," *Met. Mater. Int.,* vol. 19, no. 6, pp. 1361-1364, Jan. 2013.

[34] W. Menesklou, H.-J. Schreiner, K. H. Hardtl, and E. Ivers-Tiffee, "High temperature oxygen sensors based on doped $SrTiO_3$," *Sens. Actuators, B,* vol. 59, pp. 184–189, 1999.

[35] Z. Chao, W. Chun-Lei, L. Ji-Chao, and Y. Kun, "Structural and electronic propertiesm of Fe-doped $BaTiO_3$ and $SrTiO_3$," *Chin. Phys. Soc.,* vol. 16, no. 5, pp. 1422-1428, May 2007.

[36] F. M. Pontes, D. S. L. Pontes, A. J. Chiquito, M. A. Pereira-da-Silva, and E. Longo, "Effect of Fe-doping on the structural, microstructural, optical, and ferroeletric properties of $Pb_{1/2}Sr_{1/2}Ti_{1-x}Fe_xO_3$ oxide prepared by spin coating technique," *Mat. Let.,* vol. 138, pp. 179-183, Jan. 2015.

[37] Y. W. Li, J. L. Sun, X. J. Meng, J. H. Chu, and W. F. Zhan, "Structural and optical properties of $Ba(Co_X,Ti_{1-X})O_3$ thin films fabricated by sol-gel process," *Appl. Phys. Lett.,* vol. 85, no. 11, pp. 1964-1966, Sep. 2004.

[38] D. Maity and R. T. R. Kumar, "Highly sensitive amperometric detection of glutamate by glutamic oxidase immobilized Pt nanoparticle decorated multiwalled carbon nanotubes (MWCNTs)/polypyrrole composite," *Biosens. Bioelectron.,* vol. 130, pp. 307-314, Apr. 2019.

[39] Y. Wang, Y. Xu, L. Luo, Y. Ding, X. Liu, and A. Huang, "A novel sensitive nonenzymatic glucose sensor based on perovskite $LaNi_{0.5}Ti_{0.5}O_3$-modified carbon paste electrode," *Sens. Actuators, B,* vol. 151, pp. 65-70, Nov. 2010.

[40] R. Khan, W. Gorski, and C. D. Garcia, "Nanomolar detection of glutamate at a biosensor based on screen-printed electrodes modified with carbon nanotubes," *Electroanalysis,* vol. 23, Oct. 2011.

[41] I. Rubinstein, E. Sabatani, and J. Rishpon, "Electrochemical impedance analysis of polyaniline films on electrodes," *J. Electrochem. Soc.,* vol. 134, no. 12, pp. 3078-3083, Dec. 1987.

[42] W. Chen, S. Cai, Q.-Q. Ren, W. Wen, and Y.-D. Zhao, "Recent advances in electrochemical sensing for hydrogen peroxide: A review," *Analyst*, vol. 137, pp. 49-58, 2012.

[43] J. M. George, A. Antony, and B. Mathew, "Metal oxide nanoparticles in electrochemical sensing and biosensing: a review," *Microchim. Acta,* vol. 185,no. 7, pp. 1-26, Jul. 2018.

[44] E. M. Bauer, C. Bellitto, M. Pasquali, P. P. Prosini, and G. Righini, "Versatile synthesis of carbon-rich $LiFePO_4$ enhancing its electrochemical properties," *Electrochem. Solid-State Lett.,* vol. 7, pp. A85-A87, Feb. 2004.

[45] E. Malel and D. Mandler, "Direct electron transfer between glucose oxidase and gold nanoparticles; when size matters," *ChemElectroChem*, vol. 6, pp. 147-154, Jan. 2019.

[46] T. Ito, "Electron hopping through redox moieties anchored to well-defined nanostructures," *Chem. Rec.,* vol. 15, pp. 1148-1150, 2015.

[47] Y. Zhao, S. Chen, B. Sun, D. Su, X. Huang, H. Liu, Y. Yan, K. Sun, and G. Wang, "Graphene-Co_3O_4 nanocomposite as electrocatalyst with high performance for oxygen evolution reaction," *Sci. Rep.,* vol. 5, pp. 1-7, 2015.

[48] B. Sawicki, E. Tomaszewicz, M. Piątkowska, T. Groń, H. Duda, and K. Górny, "Correlation between the band-gap energy and the electrical conductivity in $MPr_2W_2O_{10}$ tungstates (Where M = Cd, Co, Mn)," *Acta Phys. Pol., A,* vol. 129, pp. A-94-A96, 2016.

[49] Y.-G. Wang, X.-G. Tang, Q.-X. Liu, Y.-P. Jiang, and L.-L. Jiang, "Room temperature tunable multiferroic properties in sol-gel-derived nanocrystalline $Sr(Ti_{1-x}Fe_x)O_{3-\delta}$ thin films," *J. Nanomater.,* vol. 7, no. 264, pp. 1-12, 2017.

[50] F. Haque, M. S. Rahman, E. Ahmed, P. K. Bakshi, and A. A. Shaikh, "A cyclic voltammetric study of the redox reaction of Cu(II) in presence of ascorbic acid in different pH media," *Dhaka Univ. J. Sci.*, vol. 61, no. 2, pp. 161-166, Jul. 2013.

[51] G. A. Mabbott, "An introduction to cyclic voltammetry," *J. Chem. Educ.*, vol. 60, no. 9, pp. 697-702, 1983.

[52] E. P. Randviir, "A cross examination of electron transfer rate constants for carbon screen-printed electrodes using electrochemical impedance spectroscopy and cyclic voltammetry," *Electrochim. Acta*, vol. 286, pp. 179–186, Oct. 2018.

[53] C. Neville, C. Ludlow, and B. Rieger, "Measuring postural stability with an inertial sensor: Validity and sensitivity," *Med. Devices.*, vol. 8, pp. 447-455, Nov. 2015.

[54] M. Metto, S. Eramias, B. Gelagay, and A. P. Washe, "Voltammetric determination of uric acid in clinical serum samples using DMF modified screen printed carbon electrodes," *Int. J. Electrochem.*, vol. 2019, pp. 1–8, Feb. 2019

[55] N. Shen, H. Xu, W. Zhao, Y. Zhao, and X. Zhang, "Highly responsive and ultrasensitive non-enzymatic electrochemical glucose sensor based on Au foam," *Sensors (Switzerland)*, vol. 19, no. 5, Mar. 2019.

[56] E. Kaivosoja, N. Tujunen, V. Jokinen, V. Protopopova, S. Heinilehto, J. Koskinen and T. Laurila, "Glutamate detection by amino functionalized tetrahedral amorphous carbon surfaces," *Talanta,* vol. 141, pp. 175-181, Apr. 2015.

[57] S. Chakraborty and C. R. Raj, "Amperometric biosensing of glutamate using carbon nanotube based electrode," *Electrochem. Commun.,* vol. 9, pp. 1323-1330, Jun. 2007.

[58] R. E. Özel, C. Ispas, M. Ganesana, J. C. Leiter, and S. Andreescu, "Glutamate oxidase biosensor based on mixed ceria and titania nanoparticles for the detection of glutamate in hypoxic environments," *Biosens. Bioelectron.,* vol. 52 pp. 397-402, Feb. 2014.

[59] M. G. F. Sales, C. Martins, M. F. Barroso, M. C. V. F. Vaz, M. B. P. Oliveira, and C. Delerue-Matos, "Electrochemical evaluations of glutamate at a gold electrode," *Port. Electrochim. Acta,* vol. 25, pp. 173-183, 2007.

[60] M. M. Hussain, M. M. Rahman, A. M. Asiri, and M. R. Awual, "Non-enzymatic simultaneous detection of l-glutamic acid and uric acid using mesoporous Co_3O_4 nanosheets," *RSC Advances*, pp. 80511-80521, Aug. 2016.